A Self-Adapting Flexible (SELFLEX) Antenna Array for Changing Conformal Surface Applications

Benjamin D. Braaten, *Member, IEEE*, Sayan Roy, *Student Member, IEEE*, Sanjay Nariyal, *Student Member, IEEE*, Masud Al Aziz, Neil F. Chamberlain, *Member, IEEE*, Irfan Irfanullah, *Member, IEEE*, Michael T. Reich, *Member, IEEE*, and Dimitris E. Anagnostou, *Senior Member, IEEE*

***Abstract*—A phased-array test platform for studying the self-adapting capabilities of conformal antennas is developed and presented. Specifically, a four-port 2.45-GHz receiver with voltage controlled phase shifters and attenuators is designed along with four individual printed microstrip patch antennas attached to a conformal surface. Each antenna is connected to the corresponding receiver port with a flexible SMA cable. It is shown that with appropriate phase compensation, the distorted radiation pattern of the array can be recovered as the surface of the conformal array changes shape. This pattern recovery information is then used to develop a new self-adapting flexible 1 × 4 microstrip antenna array with an embedded flexible sensor system. In particular, a flexible resistive sensor is used to measure the deformation of the substrate of a conformal antenna array, while a sensor circuit is used to measure the changing resistance. The circuit then uses this information to control the individual voltage of the phase shifters of each radiating element in the array. It is shown that with appropriate phase compensation, the radiation properties of the array can be autonomously recovered as the surface of the flexible array changes shape during normal operation. Throughout this work, measurements are shown to agree with analytical solutions and simulations.**

***Index Terms*—Adaptive antennas, conformal antennas, microstrip arrays, phased arrays and planar arrays.**

I. Introduction

FOR many years, conformal antennas have been used extensively for wireless applications that require an antenna to operate on a surface that is not flat [1]–[8] (i.e., a singly or doubly curved surface [4]). For much of this work (with the exception of [1]), it was assumed that the conformal surface was fixed (rigid) during normal operation of the antenna. This assumption is useful; however, many applications could benefit from a conformal antenna that can operate on surfaces that change shape.

Wearable antennas [9]–[17] are good examples of conformal antennas that are required to operate over a wide range of surface deformations. Only recently have textile (or wearable) antennas received considerable attention for light weight body worn applications. Results from these studies have shown that conductive textiles and unique manufacturing techniques can be used to develop antennas embedded in clothing and composite materials with 1) dual band characteristics [9], [10]; 2) ultra-wideband operation [13] and 3) load bearing capabilities [16], [17]. However, it has also been shown that conformal antennas designed for a specific surface cannot be applied to different conformal surfaces without significantly affecting the matching and radiation properties [1], [2], [4], [7], [8]. In fact, it appears that the results reported in [1] are among the first attempts to study conformal antennas on a surface that changes shape during normal operation. This early work developed a three element array consisting of horn antennas connected to a flexible steel strip. One end of the steel strip was fixed and the remaining portion consisting of the horn antennas was subjected to small spacial changes (i.e., minor surface deformations). The antenna array presented in [1] was innovative and unique; however, the mechanical and electrical limitations restricted the linear array to surfaces with only slight changes. Many modern array applications require a much smaller conformal antenna design that can autonomously adapt to conformal surfaces with many different shapes. In more recent work, field calibrations [18], [19], control circuit encoding [20], orthogonally encoded monopulse techniques [21], and beamforming [22]–[27] have been developed and presented to accurately calibrate and control the amplitude and phase of each element across an array aperture to compensate for errors caused by thermal variations (for example, seasonal variations and space-based antennas), aging effects, elemental failures, and vibrations. The work presented in [22] and [26] describe computational models to predict the radiation pattern distortion of a conformal phased-array antenna located on a deformed structure. These models are based on physical optics, incremental theory of diffraction and numerical computations of compensated array factors and take into account imperfections of antenna elements and vibrations. Furthermore, the work reported in [24], [25], and [27] describes passive structures, phase-sensing circuitry, and digital signal processing techniques

Manuscript received March 22, 2012; revised August 21, 2012; accepted October 11, 2012. Date of publication October 23, 2012; date of current version January 30, 2013. This material is based upon work supported in part by the Defense Miroelectronics Activity (DMEA) under agreement number H94003-09-2-0905, by NASA ND EPSCoR under agreement number NNX07AK91A, by the Defense Advanced Research Projects Agency (DARPA)/Microsystems Technology Office (MTO) Young Faculty Award program under Award No. N66001-11-1-4145, and in part by the Air Force Research Laboratories under contract FA9453-08-C-0245.

B. D. Braaten, S. Roy, S. Nariyal and I. Irfanullah are with the Department of Electrical and Computer Engineering, North Dakota State University, Fargo, ND 58102 USA (e-mail: benbraaten@ieee.org).

M. Al Aziz is with the Department of Electrical Engineering and Computer Science, University of Kansas, Lawrence, KS 66045 USA.

N. F. Chamberlain is with the Jet Propulsion Laboratory (JPL), California Institute of Technology, Pasadena, CA 91109 USA.

M. T. Reich is with the Center for Nanoscale Science and Engineering (CNSE), North Dakota State University, Fargo, ND 58102 USA.

D. E. Anagnostou is with the the Department of Electrical and Computer Engineering, South Dakota School of Mines and Technology, Rapid City, SD 57701 USA.

Color versions of one or more of the figures in this paper are available online at http://ieeexplore.ieee.org.

Digital Object Identifier 10.1109/TAP.2012.2226227

to control the amplitude and phase of the voltage driving the element of the conformal antenna to counteract the effects of deformation and vibrations on array antennas by means of adaptive or synthetic beamforming. The research presented in [22] and [24]–[27] provided a considerable amount of ground breaking information on how the radiation pattern of a conformal array can be distorted for various surfaces as well as circuitry for different compensation techniques; on the other hand, some of the compensation circuitry requires extensive DSP computations and RF circuitry beyond phase- and amplitude-tapering devices.

To preserve the characteristics of the antenna during operation, real-time information on the antenna topology is essential. In particular, for antenna arrays attached to a conformal surface, accurate knowledge of the surface curvature is critical, especially if the surface changes shape (i.e., curvature) with time. The objective of this work is to implement a low-cost yet accurate technique for the autonomous self-correction (i.e., without any human intervention) of an antenna array due to substrate flexing or structural strain. Furthermore, this new technique is not dependent on RF components, is achieved with minimal system complexity, and can be embedded directly into the design of an antenna array (i.e., has minimal volume requirements which are essential to spacecraft systems). This antenna differs from the aforementioned work in the sense that locally based sensors and simple analog circuitry are used to both detect and correct the effects of antenna deformations. In particular, this effort is focused on the development of an autonomously self-adapting antenna for continuously varying surface deformations with localized sensors embedded into the conformal substrate. With these features, this antenna array can thus maintain its direction of maximum radiation toward the original direction of its main beam in real-time (or toward another direction if required) when the surface that the conformal antenna is attached to changes shape.

To understand and demonstrate the self-adapting capabilities of a conformal antenna, the phased-array antenna test platform shown in Fig. 1 was initially developed. It consists of a four-port receiver and four individual microstrip patch antennas attached to each port with a flexible SMA cable. Using LabVIEW [29], the voltage controlled attenuators and phase shifters can be individually controlled on each port. This antenna system was then used to investigate the practical limitations of implementing analytical expressions for correcting the radiation pattern of a conformal array. From this information and understanding, a new self-adapting flexible microstrip patch antenna array was developed and is presented here. A schematic of the array is shown in Fig. 2. In particular, a 1×4 array with an embedded sensor network is developed on a flexible grounded substrate for conformal applications. The embedded sensor system consists of a flexible resistive sensor for measuring antenna surface deformation and a sensor circuit used to control individual phase shifters in the array. By controlling the individual phase shifters in the array in a particular manner, the radiation pattern can be autonomously recovered as the surface of the conformal antenna changes shape. For this work, the SELF-adapting FLEXible antenna array will be denoted as the SELFLEX array.

This paper is organized in the following manner. In Section II, background on radiation pattern correction (or compensation) is presented using analytical expressions. Section III presents further work on the development of the microstrip array with the four-port receiver consisting of the voltage controlled attenuators and phase shifters and the analytical results are compared to measurements of the antenna test platform on conformal surfaces with different shapes. Section IV describes the development and measurements of the 1×4 SELFLEX array. Finally, discussion on the development of both arrays and a conclusion will be presented in Sections V and VI, respectively.

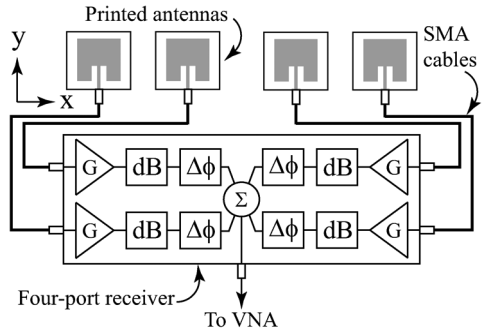

Fig. 1. Schematic of the antenna test platform.

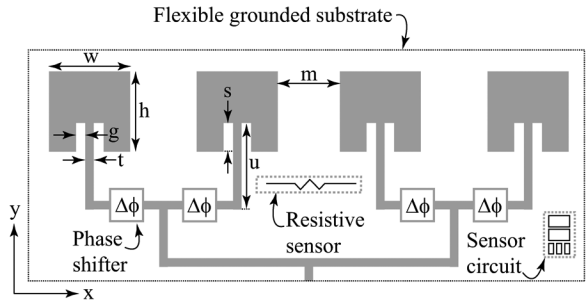

Fig. 2. Schematic of the 1×4 Self-adapting flexible (SELFLEX) array with embedded sensor circuitry.

II. Antenna Arrays on Singly Curved Surfaces

The projection method presented in [28] will be adopted for this work and will be used to describe the behavior of the conformal antenna array being developed. For discussion, consider the problem where the conformal array in Fig. 3 is bent from the flat position (original reference plane) and placed on the singly curved surface shaped as a wedge with an angle θ_w. The position of each element on the wedge is represented as a solid black dot with the outline of the surface illustrated as a black line. For this case, if each antenna element is excited with voltages that have the same phase, the E-field radiated from each element will have the same phase. However, when the fields from the elements $A_{\pm 2}$ arrive at the new reference plane,[1] the phase will be different than the fields radiated from elements $A_{\pm 1}$. This phase difference is due to the free-space propagation in the y-direction. Because these phases are not the same, the radiation may not necessarily be broadside to the array (i.e., in the z-direction with $\phi_s = \pi/2$).

[1]The new reference plane in Fig. 3 was defined only for discussion purposes. The same concepts and understanding could be applied to understand the radiation with the original reference plane. However, the new reference plane will be used for the remainder of this work.

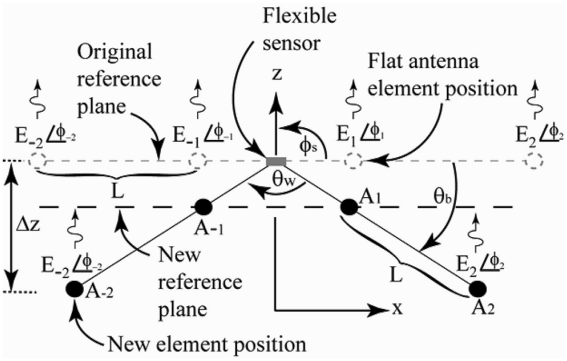

Fig. 3. Phase compensation of a linear array on a single curved surface shaped as a wedge.

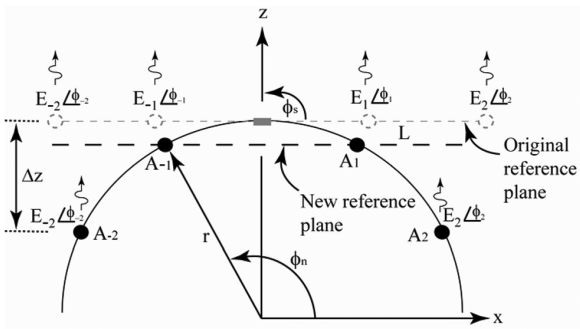

Fig. 4. Phase compensation of a linear array on a single curved surface shaped as a cylinder.

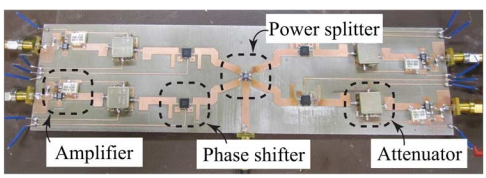

Fig. 5. Picture of the four-port receiver.

When the conformal array in Fig. 3 is attached to the singly curved surface, an x- and z-translation from the original flat position is associated with each antenna element. The amount of free-space phase introduced by the propagation of the wave from elements $A_{\pm 2}$ to the new reference plane can be computed by [4]

$$\delta_n = -k\left(|x_n|\cos\phi_s + |z_n|\sin\phi_s\right) \tag{1}$$

where k is the free-space wave number and (x_n, z_n) is the location of the n^{th} element in the linear array. As mentioned before, for this work, it is assumed that the scan angle is $\phi_s = \pi/2$. This then simplifies (1) to

$$\delta_n = -k|z_n|. \tag{2}$$

Then, using the definition of θ_w in Fig. 3, the required phase compensation can be computed as

$$\Delta\phi_n^w = +kL|n|\sin\theta_b \tag{3}$$

where $\theta_b = (\pi - \theta_w)/2$ is the bend angle of the array, the superscript w is used to denote a wedge-shaped surface, and L is the element spacing in wavelengths. The expression in (3) is the phase difference between the adjacent antenna elements required to correct the radiation pattern of the array and this expression is derived specifically for a wedge-shaped surface with a bend angle θ_b. An expression can also be derived for the curved surface in the shape of the cylinder shown in Fig. 4. By denoting the position of the n^{th} element in the array as (r, ϕ_n), the amount of required phase compensation can be computed as

$$\Delta\phi_n^c = +kr\left|\sin(\phi_n) - \sin(\phi_{n-1})\right| \tag{4}$$

where r is the radius of the cylinder. Again, the expression in (4) assumes a scan angle of $\phi_s = \pi/2$.

III. Four-Element Conformal Antenna Array Test Platform Design

The development of a 2.45-GHz conformal antenna array test platform to practically implement the phase compensation expressions (3) and (4) is presented next. In particular, the antenna test platform, shown schematically in Fig. 1, consists of a four-port receiver, four printed microstrip antennas, and four identical coaxial cables with SMA connectors to connect the antennas to the receiver. By printing individual antennas, this test platform can be used to test many different conformal antenna configurations. A picture of the manufactured four-port receiver board is shown in Fig. 5. The receiver was manufactured on a 60-mm-thick Rogers RT/duroid 6002 substrate ($\varepsilon_r = 2.94$, $\tan\delta = 0.0012$) [30].

A. Four-Port Receiver Design

The receiver in Fig. 1 consists of four input ports and a single output port. Each port has an LNA (denoted by gain G), a voltage controlled attenuator (denoted as dB), and a voltage controlled phase shifter (denoted as $\Delta\phi$) that feeds the power combiner. The LNAs (part number: PMA-545+), the voltage controlled attenuators (part number: RVA-3000+), and power combiner (part number: WP4R+) are manufactured by Mini-circuits [31], and the voltage controlled phase shifters (part number: HMC928LP5E) are manufactured by Hittite Microwave Corporation [32]. The voltage controlled attenuators and phase shifters are used to control the amplitude and phase, respectively, of the incoming signal on each individual port. In particular, the attenuators were set to the lowest attenuation value to provide the LNAs with incoming signals that have similar amplitudes. Then, the voltage controlled phase shifters were used to introduce the phase compensation computed using (3) and (4).

B. Digital-to-Analog Board Design

The voltage controlled attenuators and phase shifters in the four-port receiver were controlled individually with a Texas Instruments (TI) DAC7718S Low-power 12-bit Octal digital-to-analog converter (DAC) [33]. LabVIEW was used to communicate serially with the TI DAC to control the eight analog output voltages (channels) from 0 to 15 V.

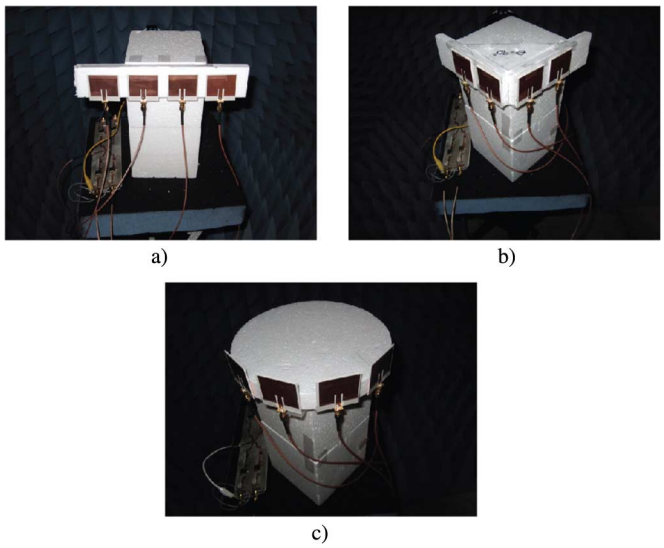

Fig. 6. a) Picture of the 1 × 4 antenna test platform attached to a nonconducting flat surface; b) picture of the 1 × 4 antenna test platform attached to a nonconducting wedge, and c) picture of the 1 × 4 antenna test platform attached to a nonconducting cylinder.

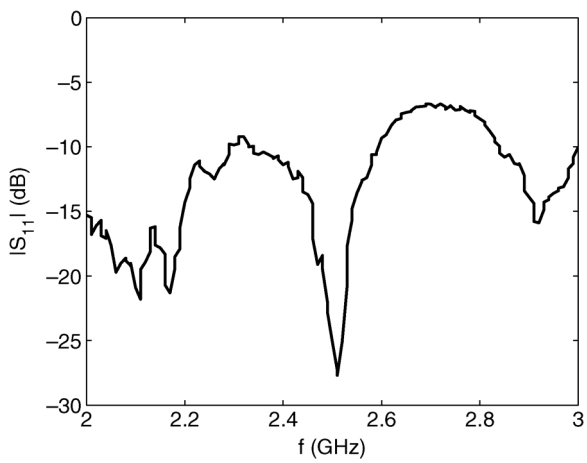

Fig. 7. Measured S_{11} of the 1 × 4 antenna test platform.

C. S-Parameter Measurements and Scanning Properties

To evaluate the performance of the antenna test platform, the antennas were initially attached to a flat surface and the S-parameters and scanning characteristics were measured. A picture of the test setup in the anechoic chamber is shown in Fig. 6(a). The antennas were designed in Momentum [34] and were manufactured on a 60-mm-thick Rogers RT/duroid 6002 substrate. The measured S-parameters at the port connected to the power combiner of the test platform are shown in Fig. 7, and a good 10-dB impedance match is observed at 2.45 GHz. Next, with an element spacing of $\lambda/2$, the scanning capabilities of the array were measured and are shown in Fig. 8 for $\phi_s = -30°$, 0° and $+30°$. Also shown in Fig. 8 are the analytically computed array patterns for a uniformly excited, equally spaced linear array (UE,ESLA) [35]. Good comparison is observed between the predicted and measured radiation patterns. These results show a good match and that the phase shifters in the four-port receiver are all operating correctly.

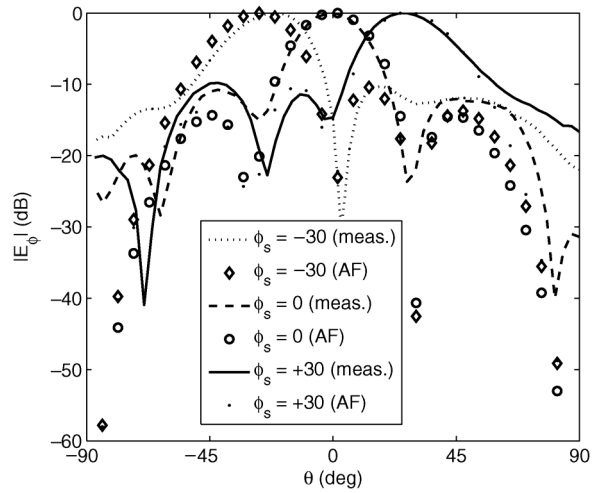

Fig. 8. Measured and analytical scanned patterns in the x–z plane for the 1 × 4 antenna test platform on a flat surface ($\theta_b = 0°$).

D. Phase Compensation and Pattern Correction Results

To implement the phase compensation expressions in (3) and (4), the antenna test platform was attached to the nonconducting wedge-shaped conformal surface shown in Fig. 6(b) and the nonconducting cylinder shown in Fig. 6(c). Then, the phase compensation values were computed analytically and the voltages on the phase shifters were adjusted manually using LabVIEW to introduce the computed phase shift compensation.

1) Analytical Computations and the Shifted Gain Values: To analytically compute the corrected (compensated) radiation pattern and validate the measurements of the antenna test platform on the conformal surfaces, the following compensated array factor (AF_c) was used:

$$\mathrm{AF}_c = \mathrm{AF} e^{j\Delta\phi_n} \tag{5}$$

where $\Delta\phi_n$ is the phase compensation term for the free-space phase delay computed using (3) and (4) and the array factor (AF) expression for antennas on conformal surfaces is [4]

$$\mathrm{AF} = \sum_{n=1}^{N} w_n e^{jk[x_n(u-u_s)+y_n(v-v_s)+z_n\cos\theta]}. \tag{6}$$

Equation (6) assumes a spherical coordinate system where $u = \sin\theta\cos\phi$, $u_s = \sin\theta_s\cos\phi_s$, $v = \sin\theta\sin\phi$, $v_s = \sin\theta_s\sin\phi_s$, θ_s is the elevation steering angle, ϕ_s is the azimuth steering angle, and w_n is the complex weighting function. For this work, an element factor of $e(\theta) = A\cos\theta$ was defined and each complex weighting function was defined as $w_n = e(\theta)e^{j\alpha}$, where α was the voltage angle used to scan the array, and the attenuator was used to control the amplitude A of each element.

A metric for determining what constitutes the pattern recovery of an antenna array is defined next. First, the reference gain $G_r(\theta,\phi)$ is defined in a certain direction for the antenna attached to a particularly defined surface. Next, the compensated gain in the same direction after the surface has been deformed and phase compensation is implemented is defined

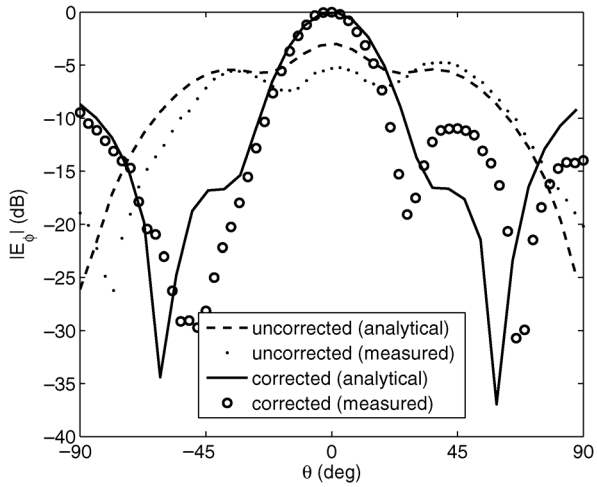

Fig. 9. Measured and analytical patterns at 2.45 GHz in the x–z plane for the 1×4 antenna test platform on a wedge with $\theta_b = 30°$.

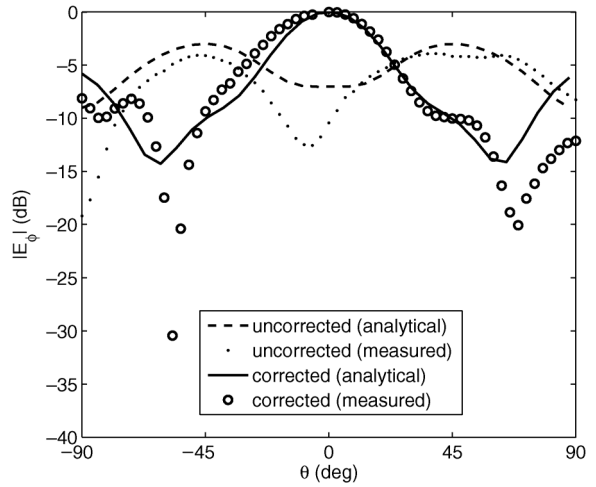

Fig. 10. Measured and analytical patterns at 2.45 GHz in the x–z plane for the 1×4 antenna test platform on a wedge with $\theta_b = 45°$.

as $G_c(\theta, \phi)$. Then, the gain shift in a particular direction due to phase compensation is defined as

$$G_s(\theta, \phi) = G_c(\theta, \phi) - G_r(\theta, \phi). \tag{7}$$

This computed gain shift value can then be compared to measurements to determine if the antenna pattern is recovered or corrected. As mentioned before, the gain broadside to the antenna will be measured, and the reference surface used to evaluate $G_r(\theta, \phi)$ is assumed to be flat ($\theta_b = 0°$).

2) Phase Compensation Results: First, the antenna test platform was attached to the wedge-shaped conformal surface in Fig. 6(b) with bend angles $\theta_b = 30°$ and 45°. Element spacing was $\lambda/2$, and the operating frequency was set to 2.45 GHz. The radiation pattern was then measured in the x–z plane for both the compensated and uncompensated cases and the results are shown in Figs. 9 and 10 for $\theta_b = 30°$ and 45°, respectively. The uncorrected results represent the case when the phase shifters are all set to the same value (i.e., same voltage) to give $\Delta\phi_n^w = 0$ and the corrected results are for the case in which the phase is advanced on elements $A_{\pm 2}$. The computed phase advance values were found using (3). By defining the new reference plane in Fig. 3 to include elements $A_{\pm 1}$, the voltage on the phase shifters feeding these elements could be fixed. This then provided a reference phase and then only the voltage on the phase shifters feeding elements $A_{\pm 2}$ had to be adjusted for phase advancement. The antenna factor terms in (5) and (6) were used next to compute the pattern of the array on both wedge-shaped conformal surfaces. In particular, the uncorrected antenna patterns were computed using (6), and these results are shown in Figs. 9 and 10, and the corrected antenna patterns were computed using (5), and these results are also shown in Figs. 9 and 10. In all cases, fair agreement between the measurements and the analytical computations can be observed.

The antenna test platform was then attached to the nonconducting cylinder shown in Fig. 6(c). The radius of the cylinder was 10 cm, the element spacing was $\lambda/2$ at 2.45 GHz and the required phase compensation was computed using (4). The measured corrected and uncorrected radiation patterns are shown to agree with the analytical results computed using (5) and (6) in Fig. 11.

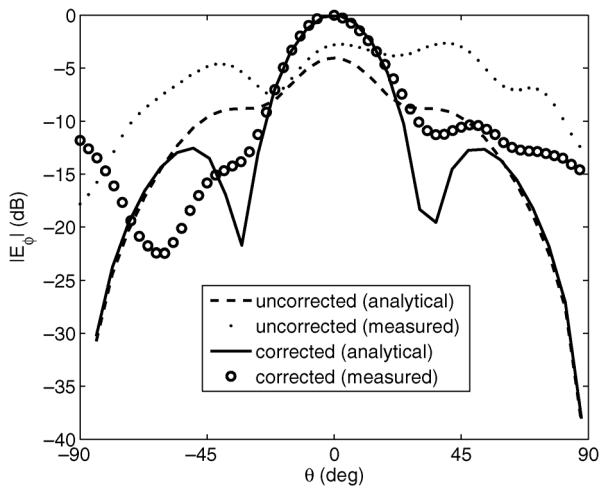

Fig. 11. Measured and analytical patterns at 2.45 GHz in the x–z plane for the 1×4 antenna test platform on a cylinder with a radius of curvature of 10 cm.

To determine the phase-compensation performance of the antenna, the measured gain shift values were compared to analytical computations. The analytical gain shift values were first computed by projecting the antenna elements in Fig. 3 for $\theta_b = 30°$ and 45° onto the x-axis with the same phase. This then resulted in a new projected linear array with a spacing of $L \cos \theta_b$. Then, using the analytical gain expressions for a linear array reported in [3], the new gain of the project array could be computed for various values of θ_b. Using the flat antenna array with an interelement spacing of $L = \lambda/2$, the reference gain was computed and then subtracted from the gain of the projected arrays for $\theta_b = 30°$ and 45°. The results from these computations are shown in the second column of Table I. Next, the calibrated gain of the array was measured in the flat position and subtracted from the calibrated gain of the compensated array for $\theta_b = 30°$ and 45°. These values are shown in the third column of Table I and agree with the analytical computations, indicating that the array is operating correctly. A negative value for the gain shift

TABLE I
GAIN SHIFT VALUES FOR THE ANTENNA TEST PLATFORM

Surface	$G_{s,analy.}$	$G_{s,meas.}$	Proj. spacing
θ_b = 30°	-0.6 dBi	-1.0 dBi	0.43λ
θ_b = 45°	-1.3 dBi	-1.8 dBi	0.35λ
Cylinder	-0.8 dBi	-1.6 dBi	non-uniform

Fig. 12. Picture of the manufactured 1 × 4 SELFLEX array prototype (g = 2.0 mm, h = 35.6 mm, m = 19.8 mm, s = 11.0 mm, t = 1.3 mm, u = 33.4 mm, and w = 43.6 mm).

was observed for each test case. This is because when the array is projected onto the x-axis for $\theta_b = 30°$ and 45°, the spacing between the elements is less than $\lambda/2$ (which was the interelement spacing for the flat case), which results in an array with less gain [36]. The projected spacing values are also reported in Table I for $\theta_b = 30°$ and 45°. Finally, the analytical gain shift is shown in Table I for the antenna on the cylindrical surface in Fig. 6(c). This analytical value was computed using the gain expressions presented in [3] for a nonuniformly spaced array. The gain shift value on the cylinder is in between the values of $\theta_b = 30°$ and 45°, which seems reasonable because 1) the overall length of the projected array is 1.29 λ, which is approximately the length of the array projected from the wedge-shaped surface with $\theta_b = 30°$ and 2) when the elements of the array on the cylinder are projected onto the x-axis, the interelement spacing is not uniform.

The results in Figs. 9–11 and Table I show that with appropriate phase compensation, an adaptive array can be developed that has a similar radiation pattern when placed on different conformal surfaces. In the following section, the techniques developed from this test platform will be adopted to synthesize a 1 × 4 SELFLEX array.

IV. FOUR-ELEMENT SELFLEX ARRAY DESIGN

The SELFLEX antenna is a new type of self-adapting conformal antenna array. The principles of conformal array compensation presented in the previous section, flexible resistive sensors and analog circuitry are combined to develop the 1 × 4 SELFLEX prototype antenna shown in Fig. 12. The SELFLEX array operates in the following manner. A flexible resistive sensor is attached to the ground plane of the SELFLEX array. This sensor changes resistance as the SELFLEX antenna changes shape (curvature). The analog sensor circuitry then measures this change in resistance and uses this information to control the phase shifters in the array. By controlling the phase shifters in the appropriate manner, the SELFLEX antenna autonomously compensates the radiation pattern for various surface deformations. The elements in the array are designed to operate at 2.47 GHz on a thin and flexible 20-mm Rogers RT/duroid 6002 substrate and have a spacing of $\lambda/2$.

A. The Resistive Sensing Circuit

The analog sensor circuit is shown in the bottom right-hand corner of the SELFLEX prototype in Fig. 12, and the schematic of the circuit is shown in Fig. 13(a). The OpAmp is an AMP04 precision single-supply instrumentation amplifier manufactured by Analog Devices [37], and the flexible resistive sensor is manufactured by Spectra Symbol [38]. For the first test case, the SELFLEX prototype is attached to the wedge-shaped conformal surface used in the previous section for the antenna array test platform. The required phase compensation can be computed analytically using (3) (which is plotted in Fig. 14 for various values of θ_b).

The sensor circuit was designed to control the phase shifters in a manner that introduces the required phase compensation for various values of θ_b. To do this, a test fixture consisting of a flexible resistor attached to a wedge-shaped conformal surface was constructed. The sensor circuit was then connected to the resistive sensor and the output control voltage $\mathrm{V_{ctrl}}$ of the circuit was connected to a prototype board consisting of a single Hittite voltage controlled phase shifter. The test fixture was then used to bend the resistive sensor at various angles of θ_b, and the phase shift was measured at 2.47 GHz using a network analyzer. The measured normalized phase shift values agree well with the analytical computations as shown in Fig. 14. Finally, the same Hititte phase shifters used in the antenna test platform in the previous section are also used in the prototype SELFLEX array design in Fig. 12.

B. S-Parameter and Pattern Measurement Results

For comparison and discussion purposes, a 1 × 4 microstrip array without phase shifters was designed, manufactured, and measured. The dimensions of the array were the same as the SELFLEX array in Fig. 12 except the feed-network had microstrip transmission lines in place of the phase shifters. The array was then placed on a flat surface (reference position) and the S_{11} values were measured to determine the resonant frequency. The measured S_{11} values are shown in Fig. 15 and a resonant frequency of 2.47 GHz was observed. The S_{11} of the array without the phase shifters will be used to show that the max gain enhancement of the SELFLEX antenna is occurring in the 10 dB BW.

Next, for the radiation pattern measurements, the SELFLEX array (with the phase shifters) was attached to a wedge-shaped conformal surface in the anechoic chamber. A picture of the test setup for $\theta_b = 30°$ is shown in Fig. 16(a), and a picture of the flexible resistor used to measure the surface deformation is shown in Fig. 13(b). The S_{11} values for $\theta_b = 30°$ and 45° are shown in Fig. 15. Measurements show that a good impedance match at 2.47 GHz is achieved for both bend angles. These

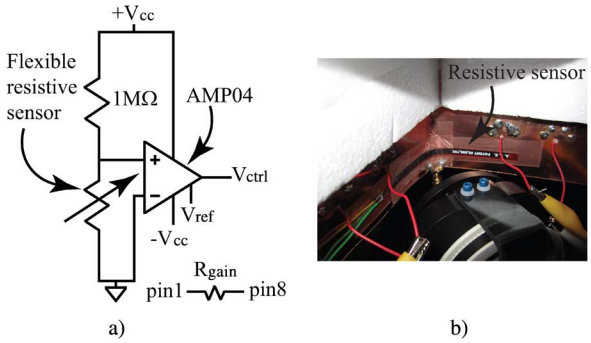

Fig. 13. a) Schematic of the sensor circuit used to measure the resistance and control the phase shifters ($V_{cc} = 15$ V, $R_{gain} = 4.7$ kΩ, and $V_{ref} = -V_{cc} = -0.4$ V) and b) a picture of the flexible resistive sensor used for measuring surface deformation.

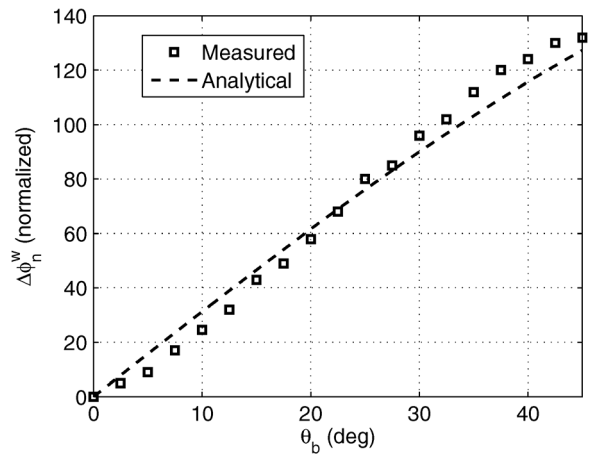

Fig. 14. Measured output of the phase shifter controlled by the sensor circuit, where θ_b is the bend angle and $\Delta\phi_n^w$ is the phase compensation for the n^{th} antenna element in the array.

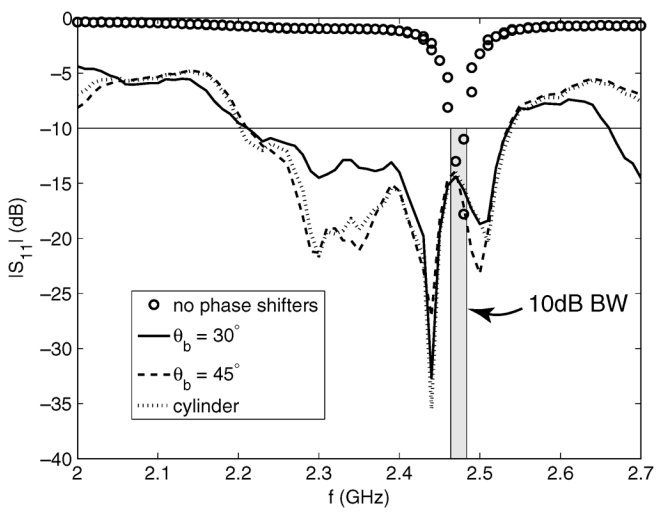

Fig. 15. Measured S_{11} of the 1 × 4 SELFLEX array for various conformal surfaces.

S_{11} values were measured with the sensor circuit controlling the phase shifters to compensate for surface curvature (i.e., the antenna is autonomously correcting the radiation pattern). The compensated and uncompensated radiation patterns were then

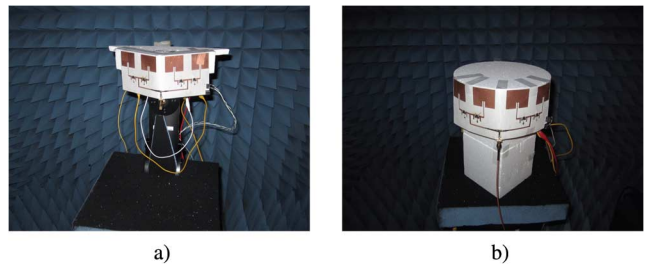

Fig. 16. a) Picture of the 1 × 4 SELFLEX array attached to a nonconducting wedge and b) picture of the 1 × 4 SELFLEX array attached to a nonconducting cylinder.

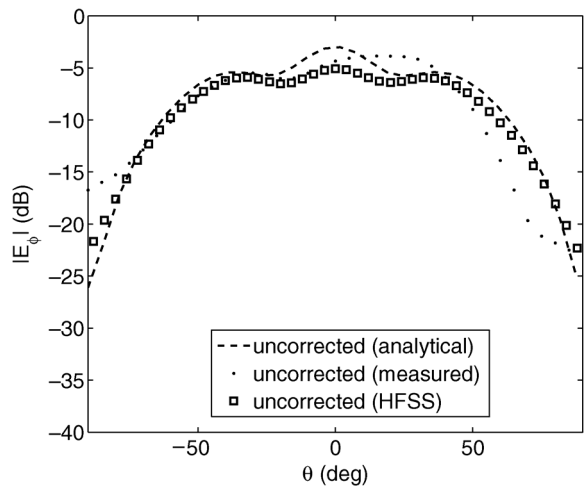

Fig. 17. Measured and analytical uncorrected patterns at 2.47 GHz in the x–z plane for the array with the embedded sensor circuit on a wedge with $\theta_b = 30^\circ$.

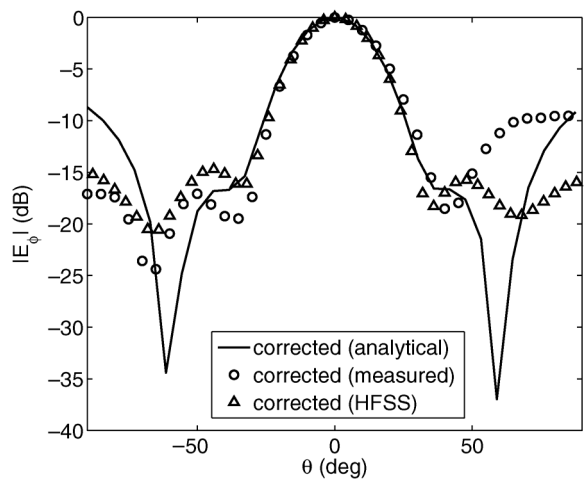

Fig. 18. Measured and analytical corrected patterns at 2.47 GHz in the x–z plane for the array with the embedded sensor circuit on a wedge with $\theta_b = 30^\circ$.

measured in the x–z plane for both bend angles. The results for $\theta_b = 30^\circ$ and $\theta_b = 45^\circ$ are shown in Figs. 17–20 at 2.47 GHz. For validation, the measured results were compared to the analytical computations using (5) and (6) and simulation results from HFSS [39]. The results from these computations and simulations are also shown in Figs. 17–20. Good agreement can be observed over the main lobe and fair agreement is shown with the sidelobes.

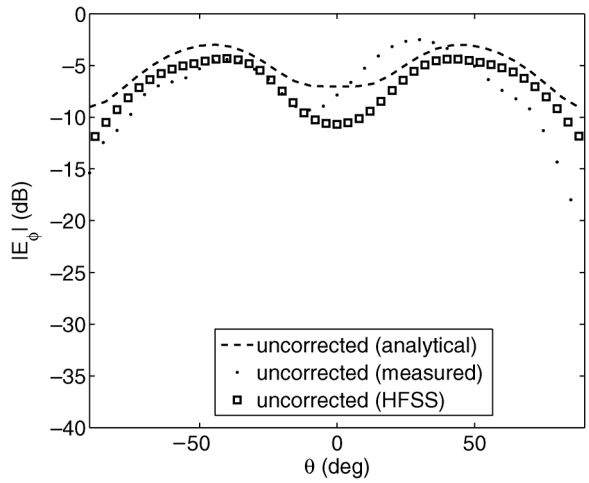

Fig. 19. Measured and analytical uncorrected patterns at 2.47 GHz in the x–z plane for the array with the embedded sensor circuit on a wedge with $\theta_b = 45°$.

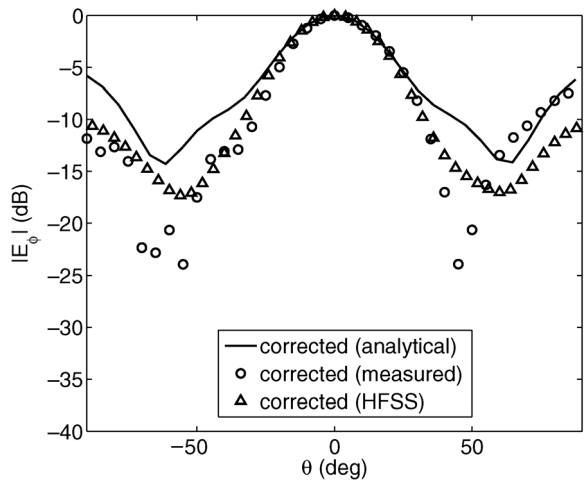

Fig. 20. Measured and analytical corrected patterns at 2.47 GHz in the x–z plane for the array with the embedded sensor circuit on a wedge with $\theta_b = 45°$.

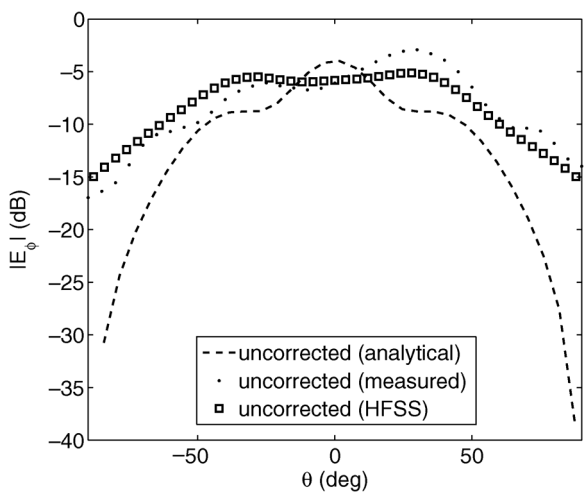

Fig. 21. Measured and analytical uncorrected patterns at 2.47 GHz in the x–z plane for the array with the embedded sensor circuit on a cylinder with a radius of curvature of 10 cm.

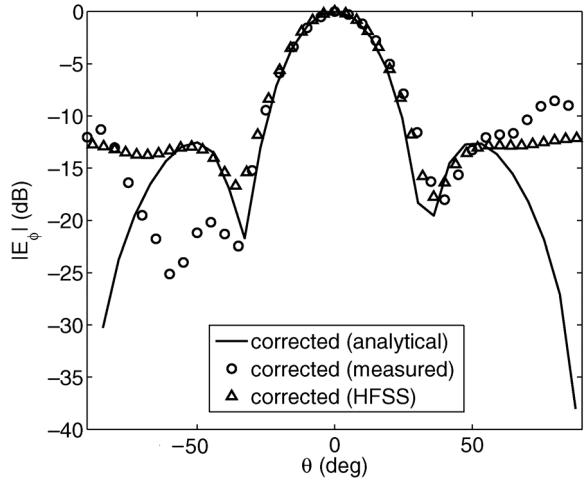

Fig. 22. Measured and analytical corrected patterns at 2.47 GHz in the x–z plane for the array with the embedded sensor circuit on a cylinder with a radius of curvature of 10 cm.

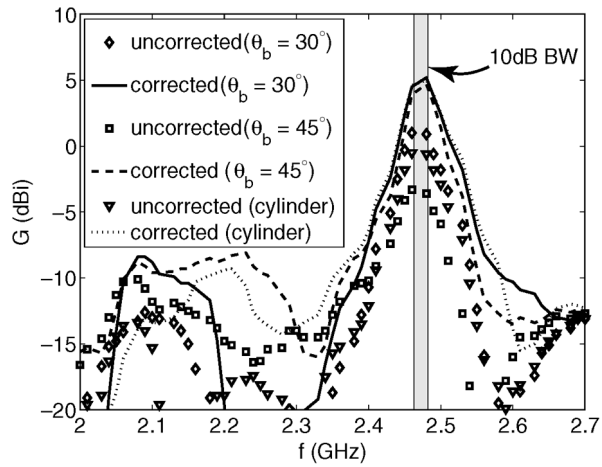

Fig. 23. Measured calibrated gain of the 1 × 4 SELFLEX array for various conformal surfaces.

TABLE II
GAIN SHIFT VALUES FOR THE SELFLEX ARRAY

Surface	$G_{s,analy.}$	$G_{s,meas.}$	$G_{s,HFSS}$	Proj. spacing
θ_b = 30°	-0.6 dBi	-0.9 dBi	-0.73	0.43λ
θ_b = 45°	-1.3 dBi	-1.4 dBi	-2.0	0.35λ
Disk	-0.8 dBi	-1.2 dBi	-1.25	non-uniform

Next, the SELFLEX antenna was attached to the conformal surface in the shape of a cylinder. Again, the radius of the cylinder was 10 cm, and a picture of the antenna being measured in the anechoic chamber is shown in Fig. 16(b). The measured S_{11} values are shown in Fig. 15 illustrating that the SELFLEX antenna has a good match at 2.47 GHz. The analytical pattern results computed using (5) and (6) and the simulated patterns in HFSS are also shown to agree well over the main lobe with the measured patterns in Figs. 21 and 22 at 2.47 GHz.

The calibrated gain values were also measured for $\theta_b = 30°$, 45° and the 10-cm disk. These results are shown in Fig. 23 for the uncorrected and corrected cases. Even though multiresonant points can be observed in Fig. 15, the results in Fig. 23 show that the improvement in the max gain (due to phase correction)

is occurring in the 10-dB BW of the antenna. It is believed that this multiresonant nature is due to the voltage controlled phase shifters not having circuitry to improve the matching. Furthermore, the measured, analytically computed, and simulated (in HFSS) gain shift values are shown in Table II, indicating a recovered radiation pattern.

The uncorrected radiation patterns shown in Figs. 17, 19, and 21 are for comparison purposes. In all cases, the radiation pattern is much broader for the uncorrected cases. These uncorrected results are similar to the results reported in [2] and [4] on circular arrays. Broadening of the array pattern is expected because the conformal antenna resembles the shape of a circular array. Overall, the main beam pattern results for the SELFLEX prototype in Figs. 17–22 compare well with the pattern results from the antenna test platform presented in Section III. Finally, it should be mentioned that the patterns were also measured in the y–z plane and were similar to the fields from a 1×4 microstrip array.

V. Overall Discussion

This work leads to the following useful results.

1) The results in Figs. 9–11 and Table I show that with appropriate phase compensation, the radiation pattern of a conformal antenna can be recovered for various surface deformations. When compared to the gain of the array on a flat surface, this pattern recovery came at the cost of only a 0.6- to 1.8-dB reduction in the overall gain of the array (i.e., the gain of the compensated array was only 0.6 to 1.8 dBi lower than the gain of the array on a flat surface with the phase shifters all set to the same value).
2) The measurements in Fig. 15 show that an autonomously self-adapting array can be developed to have good matching characteristics while being subjected to various surface deformations.
3) The radiation pattern measurements shown in Figs. 18, 20, and 22 and Table II show that a sensor circuit can be embedded into the design of a 1×4 phased-array antenna to develop a new SELFLEX antenna that can automatically recover the radiation pattern for various surface deformations.
4) The measured calibrated gain of the SELFLEX array on a flat surface was 5.9 dBi, the simulated gain (without the phase shifters) in ADS was 8.7 dBi, and the measured gain (without the phase shifters) was 8.0 dBi. This lower gain value of the SELFLEX array is expected and is due to mismatches, the 2–3-dB insertion loss of the phase shifters and the finite ground plane. The measured gain of the SELFLEX array on $\theta_b = 30^\circ$ was 5.0 dBi, on $\theta_b = 45^\circ$ was 4.5 dBi, and on the cylinder was 4.7 dBi. The gain of the SELFLEX antenna can be improved by simply inserting LNAs between the antenna elements and the phase shifters; however, since the scope of this work was to characterize and improve the radiation pattern of an antenna array using phase compensation, an LNA was not used in the design of the SELFLEX array.

VI. Conclusion

The properties and development of self-adapting conformal antennas are studied and presented in this paper. Initially, an antenna test platform was developed to practically implement analytical phase compensation values used to recover the radiation pattern of an antenna attached to various conformal surfaces. It was shown using measurements and analytical results that with appropriate phase compensation, the radiation pattern can indeed be recovered. Then, a conformal 1×4 microstrip phased-array antenna with an embedded sensor circuit was developed. The sensor circuit was used to measure the surface deformation of the conformal array and to control the phase shifters in the array. By designing the sensor circuit in an appropriate manner, it was demonstrated that this array can be attached to various conformal surfaces and autonomously preserve its radiation pattern. This novel SELF-adapting FLEXible antenna has been denoted as a SELFLEX antenna. Finally, throughout this work, measurements are shown to agree with simulations and analytical computations.

References

[1] P. L. O'Donovan and A. W. Rudge, "Adaptive control of a flexible linear array," *Electron. Lett.*, vol. 9, no. 6, pp. 121–122, Mar. 22, 1973.

[2] D. J. Chung, S. K. Bhattacharya, G. E. Ponchak, and J. Papapolymerou, "An 8×8 lightweight flexible multilayer antenna array," presented at the IEEE Antennas Propag. Soc. Int. Symp., Charleston, SC, Jun. 1–5, 2009.

[3] R. C. Hansen, *Phased Array Antennas*. New York: Wiley, 1998.

[4] R. L. Haupt, *Antenna Arrays: A Computational Approach*. Hoboken, NJ: Wiley, 2010.

[5] S. Nikolaou, G. E. Ponchak, J. Papapolymerou, and M. M. Tentzeris, "Conformal double exponentially tapered slot antenna (DETSA) on LCP or UWB applications," *IEEE Trans. Antennas Propag.*, vol. 54, no. 6, pp. 1663–1669, Jun. 2006.

[6] J.-L. Guo and J.-Y. Li, "Pattern synthesis of conformal array antenna in the presence of platform using differential evolution algorithm," *IEEE Trans. Antennas Propag.*, vol. 57, no. 9, pp. 2615–2621, Sep. 2009.

[7] M. A. Aziz, S. Roy, L. A. Berge, I. Ullah, and B. D. Braaten, "A conformal CPW folded slot antenna array printed on a Kapton substrate," presented at the Eur. Conf. Antennas Propag. (EuCAP), Prague, Czech Republic, Mar. 2012.

[8] K. Wincza and S. Gruszczynski, "Influence of curvature radius on radiation patterns in multibeam conformal antennas," in *Proc. 36th Eur. Microw. Conf.*, Sep. 10–15, 2006, pp. 1410–1413.

[9] P. Salonen, Y. Rahmat-Samii, H. Hurme, and M. Kivikoski, "Dual-band wearable textile antennas," in *Proc. IEEE Antennas Propag. Soc. Int. Symp. Dig.*, Jun. 20–25, 2004, vol. 1, pp. 463–466.

[10] S. Zhu and R. Langley, "Dual-band wearable textile antenna on an EBG substrate," *IEEE Trans. Antennas Propag.*, vol. 57, no. 4, pp. 926–935, Apr. 2009.

[11] T. F. Kennedy, P. W. Fink, A. W. Chu, N. J. Champagne, G. Y. Lin, M. A. Khayat, and M. A. , "Body-worn e-textile antennas: The good, the low-mass, and the conformal," *IEEE Trans. Antennas Propag.*, vol. 57, no. 4, pp. 910–918, Apr. 2009.

[12] F. Declercq, H. Rogier, and C. Hertleer, "Permittivity and loss tangent characterization for garment antennas based on a new matrix-pencil two-line method," *IEEE Trans. Antennas Propag.*, vol. 56, no. 8, pp. 2548–2554, Aug. 2008.

[13] M. Klemm and G. Troester, "Textile UWB antennas for wireless body area networks," *IEEE Trans. Antennas Propag.*, vol. 54, pp. 3192–3197, 2006.

[14] Y. Byram, Y. Zhou, B. S. Shim, S. Xu, J. Zhu, N. A. Kotov, and J. L. Volakis, "E-textile conductors and polymer composites for conformal lightweight antennas," *IEEE Trans. Antennas Propag.*, vol. 56, no. 8, pp. 2732–2736, Aug. 2010.

[15] J.-S. Roh, Y.-S. Chi, J.-H. Lee, Y. Tak, S. Nam, and T. J. Kang, "Embroidered wearable multiresonant folded dipole antenna for RF reception," *IEEE Antennas Wireless Propag. Lett.*, vol. 9, pp. 803–806, 2010.

[16] S. E. Morris, Y. Bayram, L. Zhang, Z. Wang, M. Shtein, and J. L. Volakis, "High-strength, metalized fibers for conformal load bearing antenna applications," *IEEE Trans. Antennas Propag.*, vol. 59, no. 9, pp. 3458–3462, Sep. 2011.

[17] Z. Wang, L. Zhang, Y. Bayram, and J. L. Volakis, "Multilayer printing of embroidered RF circuits on polymer composites," presented at the IEEE Antennas Propag. Soc. Int. Symp. Dig., Spokane, WA, USA, Jul. 3–8, 2011.
[18] E. Lier, D. Purdy, and G. Kautz, "Calibration and integrated beam control/conditioning system for phased-array antennas," U.S. Patent 6163296, Dec. 19, 2000.
[19] E. Lier, D. Purdy, J. Ashe, and G. Kautz, "An on-board integrated beam conditioning system for active phased array satellite antennas," in *Proc. IEEE Int. Conf. Phased Array Systems and Technol.*, Dana Point, CA, USA, May 21–25, 2000, pp. 509–512.
[20] D. Purdy, J. Ashe, and E. Lier, "System and method for efficiently characterizing the elements in an array antenna," U.S. Patent 2002/0171583 A1, Nov. 21, 2002.
[21] E. Lier, M. Zemlyansky, D. Purdy, and D. Farina, "Phased array calibration and characterization based on orthogonal coding: Theory and experimental validation," in *Proc. IEEE Int. Symp. Phased Array Syst. Technol. (ARRAY)*, Oct. 12–15, 2010, pp. 271–278.
[22] H. Schippers, G. Spalluto, and G. Vos, "Radiation analysis of conformal phased array antennas on distorted structures," in *Proc. 12th Int. Conf. Antennas Propag. (ICAP)*, Mar. 31–Apr.. 3, 2003, pp. 160–163.
[23] H. Schippers, J. Verpoorte, P. Jorna, A. Hulzinga, A. Meijerink, C. Roeloffzen, R. G. Heideman, A. Leinse, and M. Wintels, "Conformal phased array with beam forming on airborne satellite communication," in *Proc. Int. ITG Workshop Smart Antennas*, Feb. 26–27, 2008, pp. 343–350.
[24] H. Schippers, P. Knott, T. Deloues, P. Lacomme, and M. R. Scherbarth, "Vibrating antennas and compensation techniques research in NATO/RTO/SET 087/RTG 50," in *Proc. IEEE Aerosp. Conf.*, Mar. 3–10, 2007, pp. 1–13.
[25] P. Jorna, H. Schippers, and J. Verpoorte, "Beam synthesis for conformal array antennas with efficient tapering," presented at the 5th Eur. Workshop Conformal Antennas, Bristol, U.K., Sep. 11–12, 2007.
[26] P. Knott, "Deformation and vibration of conformal antenna arrays and compensation techniques," in *Meeting Proc. RTO-MP-AVT-141*, 2006, pp. 1–12, Paper 19.
[27] T. J. Seidel, W. S. T. Rowe, and K. Ghorbani, "Passive compensation of beam shift in a bending array," *Prog. Electromagn. Res.*, vol. 29, pp. 41–53, 2012.
[28] I. Chiba, K. Hariu, S. Sato, and S. Mano, "A projection method providing low sidelobe pattern in conformal array antennas," in *IEEE Antennas Propag. Soc. Int. Symp. Dig.*, Jun. 26–30, 1989, pp. 130–133.
[29] National Instruments Corporation [Online]. Available: www.ni.com
[30] Rogers Corporation [Online]. Available: www.rogerscorp.com
[31] Mini-Circuits [Online]. Available: www.minicircuits.com
[32] Hitite Microwave Corporation [Online]. Available: www.hittite.com
[33] Texas Instruments, Inc. [Online]. Available: www.ti.com
[34] Advanced Design System (ADS) by Agilent Technologies [Online]. Available: www.agilent.com
[35] W. L. Stutzman and G. A. Thiele, *Antenna Theory and Design*, 2nd ed. New York: Wiley, 1998.
[36] J. P. Daniel, "Directivity of linear microstrip arrays," *Electron. Lett.*, vol. 23, no. 17, pp. 897–899, Aug. 1987.
[37] Analog Devices [Online]. Available: www.analog.com
[38] Spectra Symbol [Online]. Available: www.spectrasymbol.com
[39] Ansys, Inc., Ansoft HFSS, ver. 13.0.1 [Online]. Available: www.ansoft.com

Benjamin D. Braaten (S'02–M'09) received the Ph.D. degree in electrical engineering from North Dakota State University, Fargo, ND, USA, in 2009.

During the fall semester 2009, he held a postdoctoral research position at the South Dakota School of Mines and Technology, Rapid City, SD, USA. Currently, he is an Assistant Professor in the Electrical and Computer Engineering Department at North Dakota State University. His research interests include printed antennas, conformal self-adapting antennas, microwave devices, topics in EMC, and methods in computational electromagnetics.

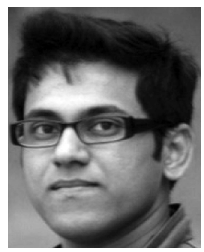

Sayan Roy (S'10) was born in Chandannagar, India, in 1988. He received the B. Tech. degree in electronics and communication engineering from West Bengal University of Technology, Kolkata, India, in 2010 and the M.S. degree in electrical and computer engineering from North Dakota State University, Fargo, ND, USA, in 2012.

Currently, he is working toward the Ph.D. degree in electrical and computer engineering at North Dakota State University, Fargo, ND, USA. His research interests include microwave antennas, printed antenna array, conformal self-adapting antennas, RFID, and topics in EMC and wearable antennas.

Sanjay Nariyal (S'06) received the B.S. degree in electrical engineering from North Dakota State University, Fargo, ND, USA, in 2010.

Currently, he is working toward the M.S. degree in electrical engineering and is a Graduate Teaching Assistant in the Electrical and Computer Engineering Department at North Dakota State University. His research interests include antennas and issues in electromagnetic compatibility.

Masud Al Aziz received the B.Sc. degree from the Bangladesh University of Engineering and Technology, Bangladesh, and the M.Sc. degree from North Dakota State University, Fargo, ND, USA.

Currently, he is working toward the Ph.D. degree at the University of Kansas, USA. His research topic is ultra-wideband antenna array design for RADAR and signal processing for ice sheet detection.

Neil F. Chamberlain (S'86–M'90) received the B.Sc. degree (with Hons.) from Kings College London, U.K., in 1981 and the Ph.D. degree in electrical engineering from The Ohio State University in 1989.

He worked briefly for Marconi Space and Defense Systems, Ltd., Portsmouth, U.K., before undertaking graduate studies at The Ohio State University. He was a Professor at the South Dakota School of Mines and Technology, Rapid City, SD, USA, between 1990 and 2003. His research focused on ultra-wideband radar antennas and systems. He is currently a Senior Engineer with the Jet Propulsion Laboratory's Spacecraft Antennas Group, where he was recently involved in developing antenna arrays for UAVSAR and Juno Microwave Radiometer Instrument. He is currently leading the antenna development for the proposed DESDynI synthetic aperture radar instrument.

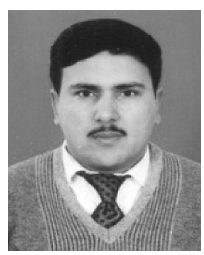

Irfan Irfanullah (S'05–M'07) received the M.S. degree in electrical engineering from the University of Engineering & Technology, Lahore, Pakistan, in 2007.

He is currently working toward the Ph.D. degree in conformal smart antennas at the North Dakota State University, Fargo, ND, USA. His research interests include the antenna arrays and topics in EMC.

Michael T. Reich (M'90) was born in Jamestown, ND, USA, in 1966. He received the B.S. degree from North Dakota State University (NDSU), Fargo, ND, USA, in 1990, the M.S. degree from The Pennsylvania State University, State College, PA, USA, in 1998, and the Ph.D. degree from NDSU in 2009, all in electrical engineering.

From 1990 to 1997, he was an Electronics Engineer with the Naval Undersea Warfare Center Keyport, where he worked with antisubmarine warfare fire control systems. From 1997 to 2005, he was a Senior Engineer at Phoenix International Corporation (now John Deere Electronics Systems), where he performed a variety of functions, including software design, project management, and EMI/EMC testing. Since 2005, he has been a Senior Research Engineer with the Center for Nanoscale Science and Engineering at NDSU, where he works on wireless sensors, RF systems, and antennas. He is also an Adjunct Professor in the NDSU Electrical and Computer Engineering department. His research interests include radio-frequency identification (RFID) systems, tunable materials for RF applications, and modification of antenna parameters through the use of novel materials.

Dr. Reich is a licensed Professional Engineer in the state of Washington.

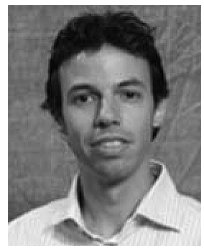

Dimitris E. Anagnostou (S'98–M'05–SM'10) received the B.S.E.E. degree from the Democritus University of Thrace, Greece, in 2000, and the M.S.E.E. and Ph.D. degrees from the University of New Mexico in 2002 and 2005, respectively.

From 2005 to 2006, he was a Postdoctoral Fellow at the Georgia Institute of Technology, Atlanta, GA, USA. Since 2007, he has been an Assistant Professor of Electrical and Computer Engineering at the South Dakota School of Mines and Technology, Rapid City, SD, USA. He has published 70 peer-reviewed journal and conference papers. His interests include reconfigurable, autonomous, flexible, electrically-small and miniaturized antennas and arrays, analytical design methods for antennas and microwave components, metamaterial applications, direct-write, "green" and Paper RF electronics, applications of artificial dielectrics and dielectric superstrates, leaky-wave antennas, cavity resonance antennas, antennas on PV-cells, RF-MEMS, propagation in tunnels, and microwave packaging.

Dr. Anagnostou was the recipient of the 2011 DARPA Young Faculty Award and the 2010 IEEE Antennas and Propagation Society (AP-S) John Kraus Antenna Award. He also received the 2011 AFRL Summer Faculty Fellowship by the ASEE. In 2006, he was recognized as a distinguished scientist living abroad by the Hellenic Ministry of Defense. He holds one patent on reconfigurable antennas. He serves as Associate Editor for the IEEE TRANSACTIONS ON ANTENNAS AND PROPAGATION and the Springer *International Journal of Machine Learning and Cybernetics*, as a member of the TPC and Session Chair for IEEE Antennas and Propagation International Symposia, and as a reviewer for 14 international publications, including IEEE T-AP, T-MTT, AP-S Magazine, AWPL, and MWCL. He has given two workshop presentations at IEEE AP-S and IEEE MTT-S International Symposia. He is a member of Eta Kappa Nu, ASEE, and of the Technical Chamber of Greece.